Maejo International Journal of Energy and Environmental Communication

Journal homepage: https://ph02.tci-thaijo.org/index.php/MIJEEC

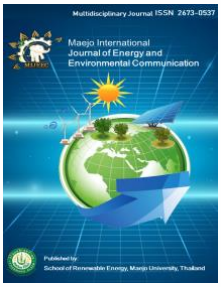

ARTICLE

Corrosion analysis of API X70 steel in seawater environment

Abdulrahman Bala Gambo[1,*], Oluwafemi Ayodeji Olugboji[1], Oyewole Adedipe[1], Joseph B. Agboola[2], Aisha Yahaya Ndanitsa[3] Sadiq Sius Lawal[4], Sunday Albert Lawal[4]

[1]Department of Mechanical Engineering, School of Infrastructure, Process Engineering and Technology, Federal University of Technology Minna, Nigeria
[2]Department of Metallurgical and Materials Engineering, University of Lagos, Nigeria
[3]Department of Economics, Nile University of Nigeria, Nigeria
[4]Department of Mechanical Engineering, School of Infrastructure, Process Engineering and Technology, Federal University of Technology Minna, Nigeria

ARTICLEINFO

Article history:
Received 24 December 2024
Received in revised form
21 January 2025
Accepted 25 January 2025

Keywords:
Corrosion
Seawater
X70 steel
Test rig
Pipelines
Marine environments

ABSTRACT

This study is designed to understand the corrosion and the mechanical properties of API X70 steel in a simulation of seawater. A special machine was built to simulate the corrosion of marine pipelines. The elemental structure and microscopic properties of the steel were identified with the help of spectroscopy and microscopy. Tests were conducted on welded samples for tensile strength, impact, compression, and hardness, first in air and again after being in seawater for twelve months. The equipment used for testing was a scanning electron microscope (SEM) to observe the fracture surfaces. It was found that the mechanical properties of API X70 steel became less resistant after being exposed to seawater. When tested in seawater, parent and weld materials had a yield strength of around 428 MPa and 416 MPa, which was a decrease from 560 MPa and 578 MPa in air. For the parent metal and the weld joint, tensile strengths were 634 MPa and 674 MPa, as compared to 512 MPa and 529 MPa afterward. Tests conducted on parent metal produced higher Charpy impact properties than HAZ and weld, and the lowest were found in seawater. Being in saltwater lowered the rigidity and toughness of the bones. Tests exposed brittle as well as ductile types of failure in SEM. The reductions in tensile strength due to the environment were 1.2-1.3, and those for impact were higher at 2.0. This information shows API X70 steel can be applied offshore and helps researchers understand how to handle corrosion better.

1. Introduction

Marine engineers have to place a high emphasis on preventing seawater corrosion to steel since today's environmental problems make such protection necessary (Lawal et al., 2024). As a result of climate change, the temperature of the oceans has gone up and acidity has increased, which causes electrochemical corrosion to develop faster in submerged metals. Besides, sea level rise adds

* Corresponding author.
E-mail address: danbauranborgu@gmail.com ; abgambo@futminna.edu.ng (Gambo A. B.)

extra loads and pressure to offshore structures due to increased waves (López et al., 2024). Entering our seas, more plastic waste, oil, and untreated wastewater are causing many problems (Behera et al., 2021; Bhuyar et al., 2020; Govindan et al., 2020), including rotting marine growth and increasing microbially influenced corrosion (MIC). Besides, when the runoff from farms adds too many nutrients to coastal waters, it promotes eutrophication that helps sulfate-reducing bacteria erode steel structures aggressively (Suliman et al., 2020). When water in certain zones becomes low in oxygen and remains stagnant, it adds to high levels of corrosion. Most of these stressors are linked to human activities and are leading to the quick destruction of offshore infrastructure (Xia et al., 2018a,b).

This has turned challenges from corrosion into bigger problems concerning sustainability and caring for the environment (Sabarikirishwaran et al., 2023). Especially for applications underwater, API X70 is commonly selected because it balances high strength, toughness, being easy to weld, and being affordable (Lawal et al., 2024). It can still suffer from long-term effects of strong seas, especially when exposed to changes in seawater rich in chemicals for a long time. Since regulations are getting tougher and people need energy that lasts, we need to make sure pipeline materials like API X70 are tough, environmentally friendly, and able to withstand ecological dangers. The carbon content in earlier production grades, especially X42 and X52, was excessive, so the welding process was unstable, and these plates did not have enough strength. For this reason, they would not work in highly stressful locations (Bott, 2024). Later, people in metallurgy reduced the carbon content and started to include vanadium (V), niobium (Nb), titanium (Ti), boron (B), and silicon (Si) to strengthen steel, make it transform differently, and decrease the chance it would crack (Louhenkilpi, 2020).

Recognizing these changes, API X70 steel was introduced, and it turned out to be a useful grade in undersea pipelines because of its strong yield, toughness, and ease of welding. The plastic material used in API X70 is normally created with ferrite and pearlite mixed, so it becomes flexible and able to distribute stress uniformly (Hwang et al., 2005). API X80 and X100 grades that mainly have ferrite–bainite and bainitic structures are selected for tougher uses. In spite of everything, making the steel tougher also makes it less flexible when being welded, so this process explains why X70 is used for shipbuilding, oil tanks, short-use bridges, marine risers, and subsea pipelines (Seth, 2024). Steel that is exposed to seawater is damaged most due to oxidation and reduction reactions. When something is anodically oxidized, iron loses electrons to end up as ferrous ions, and during the cathodic reaction, oxygen and water are reduced to hydroxide ions. The key electrochemical steps involved in steel corrosion in seawater are expressed as:

$$Fe \rightarrow Fe^{2+} + 2e^{-}$$
$$H_2O + \tfrac{1}{2}O_2 + 2e^{-} \rightarrow 2OH^{-}$$
$$Fe^{2+} + 2OH^{-} \rightarrow Fe(OH)_2$$

In steel electrolysis, the anodic dissolution of steel enables it to lose electrons and become iron hydroxide, which can dry to create rust. Because of salt, oxygen changes, water temperature, water agitation, and microbes in seawater, corrosion may increase, and the problem becomes hard to handle (Abed, 2021). Material corrosion and its type depend on what the material is, the conditions nearby, and the mechanical stress it experiences. Experts organize corrosion into three groups, and uniform corrosion belongs to that category – it can be predicted and leads to significant material loss.

Some types of localized corrosion include pitting, crevice corrosion, galvanic corrosion, erosion-corrosion, and MIC, and these can easily result in parts breaking down. This may result in existing cracks in high-strength steels getting bigger due to the pressure and effects of stress corrosion cracking (SCC) and corrosion fatigue (Ujjwal et al., 2024). Generally, localized corrosion begins secretly and only becomes obvious once the damage has become severe. Crevice corrosion in marine pipes happens due to poor fitting, but sacrificial anodes cause galvanic corrosion since different metals are used in contact. When bacteria called sulfate-reducing bacteria grow in non-flowing areas, they cause corrosion (Sabarikirishwaran et al., 2023).

During testing for corrosion in a lab, safety experts create a model of sea conditions by managing water salinity, temperature, water velocity, and the level of oxygen. After exposure tests, any modifications in the steel's qualities are carefully examined. Steel in places affected by corrosion loses strength and is likely to develop cracks. Evaluation done at a laboratory rig costs less than evaluation out in the field. It would be useful to examine the effects of both environmental changes and stress on people. People can use cathodic protection and resistant coatings as prevention methods for corrosion. All parts of the ocean have different mixtures of chemicals, pH, and temperatures (Behera et al., 2021; Bhuyar et al., 2020; Govindan et al., 2020). There are many different regions, such as splash zones, tidal areas, banks of mud, shallow areas as well as the deep ocean sea that require different types of protection.

The sea covers about 71% of the planet, and it contains about 3.5% sodium chloride. In most cases, corrosion studies use a solution of sodium chloride with a higher level of concentration (Hwang et al., 2005). Since 21 investigators are required for corrosion tests, it may be costly since anything that impacts the corrosion process will change the other parameters (Abed et al., 2021). Tests are performed depending on both the environment and the level of stress at the site. A rapid technique is used to foresee corrosion because it is cheaper. Most of the time, natural seawater is applied, and if artificial seawater is needed, it is made according to the ASTM D1141 standards. The most common parts of research are soaking tests, during which samples remain in seawater for a particular period (López et al., 2024). According to the situation, seawater can either be changed, move somewhere else, or stay as it is. Engineers look at the weight, looks, and toughness of materials as they are being tested in use. The investigation decided to simulate in-ocean conditions with seawater instead of trying other available options. Its behaviour in seawater is observed so that you can use the best materials and manage offshore pipelines effectively.

2. Materials and methods

2.1 Material

This investigation mainly relies on a 600 x 150 x 20.8 mm API X70 steel plate. The manual metal arc welding was done at SCC Nig. Ltd. in Ushafa, Bwari, and FCT Abuja. The researchers used many pieces of equipment and materials like a corrosion rig, a chiller, thermometers, pumps, a pH meter, digital microscopes, a tensile test machine, an Izod impact test machine, a Vickers hardness machine, a grinding and polishing machine, a scanning electron microscope (SEM), X-ray fluorescence, and X-ray diffraction machines for this study (Figure 1).

Figure 1. Water circulation pump (A), digital thermometer (B), digital pH meter (C), and IR thermometer (D) are used in the corrosion rig to help collect the necessary data.

2.2 Material Characterization and Spectroscopic Analysis of API X70 Steel

Characterization and Spectroscopic Analysis with the API X70: At Oshogbo Machine Tools, they use chemical analysis to determine the chemical composition of the steel plate. Spectroscopy was carried out to determine the elements and types of materials present in the steel (Figure 2).

Figure 2. Surface of API X70 steel sample after chemical and spectroscopic analysis

2.3 Microstructure examination of the test sample

The sample from the API X70 steel plate was made by applying common metals process. The sample was ground up to 1200 grit with silicon carbide papers, polished using alumina slurry, and cleaned with ethanol. After this, etching with 2% Nital solution was done to see the microstructure. The optical microscope revealed that grains are uniform and there are potential defects as well. The analysis showed the presence of ferrite-pearlite and the appearance of the sample's surface. The sample was examined at magnifications between 100× and 500× to check the grain boundaries (Figure 3), how ferrite and pearlite are spread, and any defects in the microstructure.

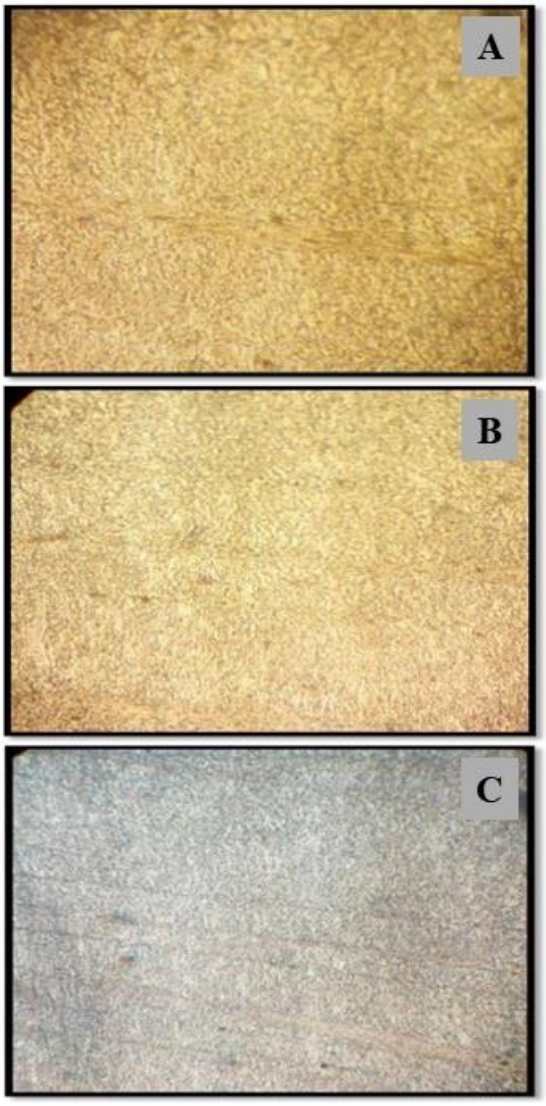

Figure 3. Optical micrographs of the API X70 steel sample at different magnifications (A–C)

2.2 Weld material and sample preparation

The steel was analyzed using spectroscopy, and then it was welded at the SCC facility in Abuja. The plates were both cleaned with a machine and with chemicals to get rid of any contaminants. The butt joint in this model has a 60° groove angle and a root thickness of 6 mm with a space between the joint of 0.3 mm, which falls within normal practice for thick-wall pipe steels (Figure 4). This setup made the welds better and limited the number of mistakes. Alignment, the preparation of each edge, and cleanliness

were kept to help the experiments be the same and to follow the rules. The samples were checked for their structure, how hard or soft they were, and their resistance to corrosion.

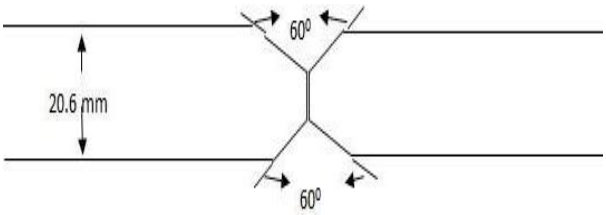

Figure 4. Schematic diagram of the double-V butt weld joint configuration

2.3 Extraction of test samples

Samples from tensile, compression, impact, and hardness tests were cut from three different areas of the welded APIX70 steel plate (the weld zone, heat-affected zone (HAZ), and parent metal. It helped to review the performance of structures exposed to welding. First, the specimens were cut with an abrasive cutter, and then they were processed using CNC technology to the standard sizes given by ASTM guidelines. As a result of grinding, polishing, and etching, surfaces were even and ready for testing and analyzing the materials' structure with reliable accuracy.

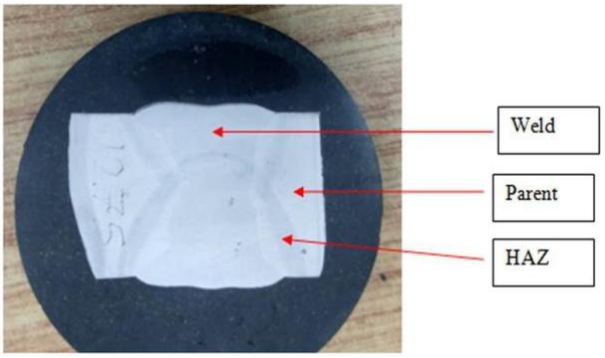

Figure 5. Macrograph showing weld zones of the API X70 steel joint

2.4 Tensile test

Stress testing was done to observe how API X70 steel samples operated in regular air and in seawater (Figure 6). By following ASTM E8/E8M rules, the tests used dog-bone specimens from weld metal, HAZ, and parent material. The samples chosen were put in synthetic seawater to see how corrosion could degrade them. To test, the universal testing machine (UTM) was used, and the ultimate tensile strength (UTS), yield strength (YS), elongation at break, along with the modulus of elasticity, were recorded. The curves showing stress against strain were studied to observe how each area of the weldment reacted to being in a marine environments.

2.5 Impact tests

The toughness of API X70 steel under dynamic loads was checked by impact testing that followed the standards from ASTM E23. From every location of interest in the samples, standard Charpy V-notch specimens were taken for testing. Every fracture was done using a pendulum impact tester, and the measurements of the fracture energy were saved. They added insight into the material's possible brittle failure after it was put into marine environments. Impact tests were done on API X70 steel by using the apparatus based on ASTM E23 standards. The quantity is obtained by knowing how much energy is taken up during bone fracture at high rates of strain (Figure 7).

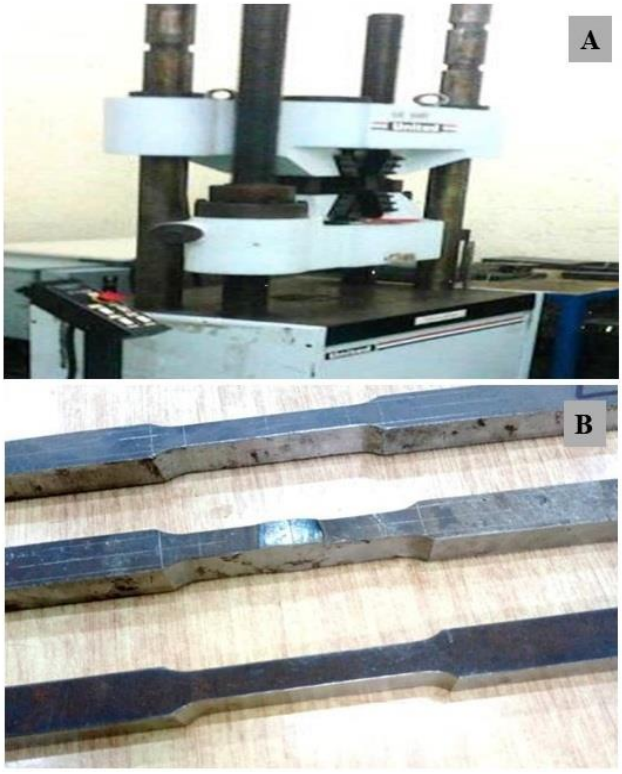

Figure 6. Tensile testing setup for API X70 steel: (A) UTM for tensile tests per ASTM E8/E8M standards and (B) Standard tensile specimens from weld zone, HAZ, and parent material of steel plate

Figure 7. Charpy impact testing machine used for toughness evaluation

2.6 Compression tests

The Instron Universal Testing Machine was used to run compression tests on the API X70 steel to see how strong it could withstand pressure and its behavior when deformed. Cylindrical samples were inserted axially along the guide, and data about load–load-load-load-load-load-load-displacement values were collected continuously (Figure 8). These tests gave me useful information on how the material behaves when it is being compressed. To look at the compressive properties of regular API X70 steel, the equipment was used to load samples axially.

Figure 8. Computerized Instron Universal Testing Machine used for compression testing

2.7 SEM analysis

The interior of some cracked samples was studied by using Scanning Electron Microscopy (Figure 9). At different magnifications, the analysis provided clear images of the microstructure, so it was possible to closely study the fractures, how the grains connect, and any possible micro-imperfections present. It made it possible to detect how corrosion and mechanical stress caused changes in a metal surface.

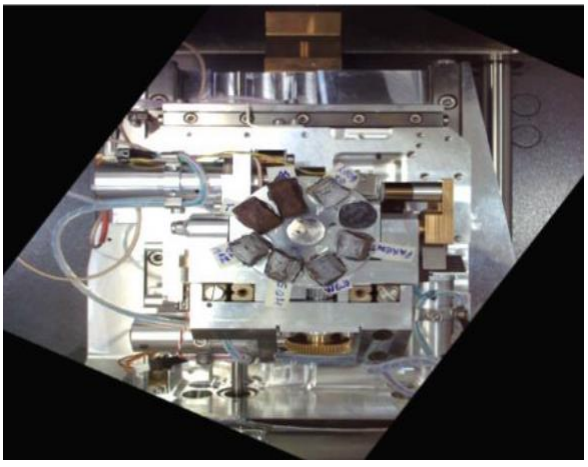

Figure 9. Computerized Instron universal testing machine used for compression testing

2.8 Hardness testing and X-ray characterization

The hardness was evaluated by ASTM E384 and API 5L/ISO 3183 standards with the use of a Vickers microhardness tester. Hardness was measured in several points across the parent metal, HAZ, and weld metal sections to notice how welding influences the hardness. Each layer was equally spaced so as not to interfere, and the results gave information about how strong the material was in different places as well as its possible vulnerability to cracking or stretching. To determine the precise composition of the steel and its structural phases, X-ray Diffraction (XRD) and X-ray Fluorescence (XRF) testing were done. XRD helped to distinguish crystalline phases and find out if any changes in the microstructure had occurred because of welding or corrosion. Using XRF analysis, it was confirmed that the API X70 sample was precisely the same alloy throughout all the weld zones and complemented the earlier spectroscopic results.

2.9 Development of corrosion rig and chilling unit

A corrosion machine was created by using materials available locally so that it mimics the marine environment for subsea pipe testing. A test was carried out at the Niger River Basin laboratory to ensure that the water taken from Lagos Lagoon was not corrosive. Using the immersion method, samples of API X70 steel were put in seawater for a year. During the test period, the solar system of 1.5 kVA was dependable for the rig to work properly. After being exposed, the samples were analyzed with weighing, visual observations, and the use of mechanical techniques to check for wear and tear. Because of this arrangement, researchers were able to discover how the API X70 steel behaves under corrosion conditions in seawater. The image in Figure 10 presents the scheme for setting up the corrosion rig, which contains a chilling unit. The left-hand side exhibits the corrosion rig made with local resources and protected by a solar energy setup for work in seawater. The illustration in the right section demonstrates how an integrated vapor compression cycle maintains the proper temperature inside the rig. The system has important elements: compressor (1), condenser (2), capillary tube (3), and evaporator (4).

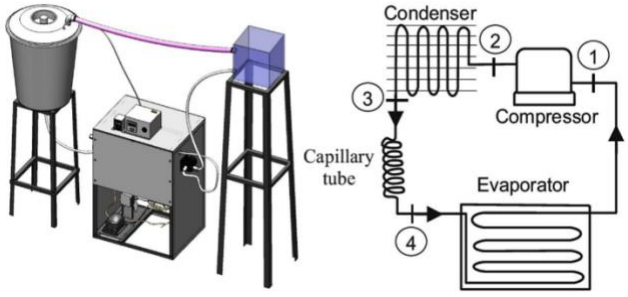

Figure 10. Computerized Instron Universal Testing Machine used for compression testing

3. Results and discussion

3.1 Microstructure Examination

Figure 11 highlights the changes that occurred to API X70 steel samples after being placed in seawater for 12 months. Traces of corrosion visible by a ferrite-pearlite structure could be recognized by them (Ike et al., 2018). It became clear that the climate inside the weld made a mix of patterns, some rough surface, micro holes from temperature changes, and a coarse-grain ferrite—wildman structure, which is easily vulnerable to localized corrosion (Adedipe et al., 2023; Song et al., 2024).

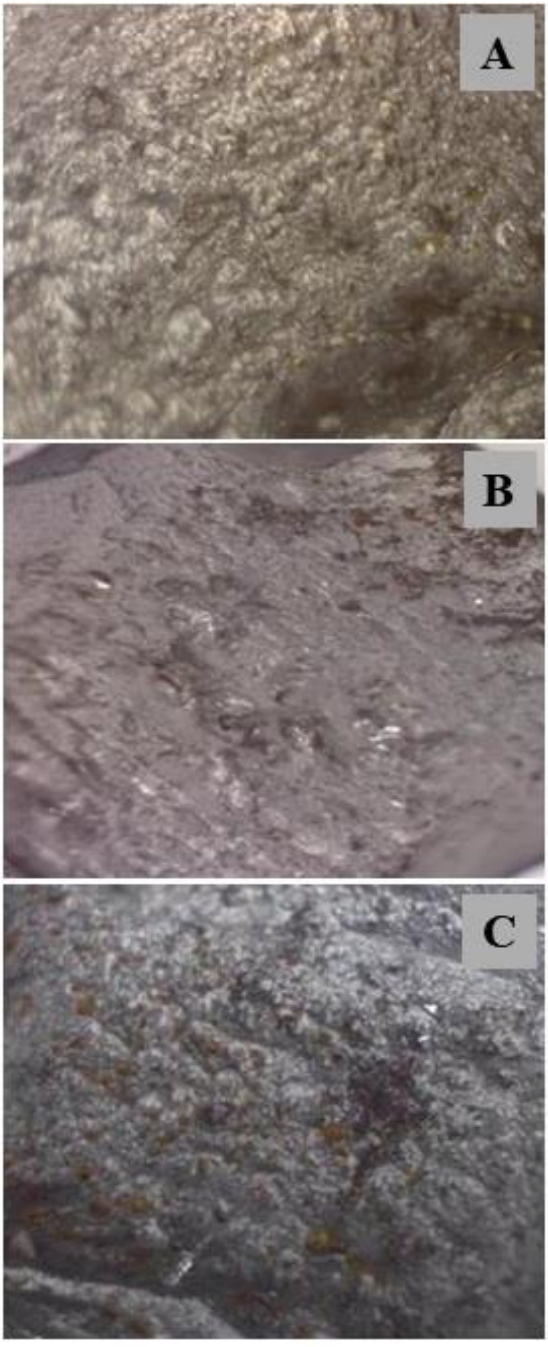

Figure 11. Optical micrographs of API X70 steel at different regions after corrosion exposure: (A) Parent material, (B) Weld zone, and (C) Heat-Affected Zone (HAZ)

Deformations showed severe damage on the HAZ, resulting mainly from microstructural unrest and grain coarsening (Adedipe et al., 2015). Several studies prove that welded joints in the HAZ tend to be more vulnerable because of incomplete transformation and structural inhomogeneity (Akonyi et al., 2020). The presence of martensite and austenite in the structure may give rise to galvanic cells and hence lead to pitting corrosion (Aliu, 2012). It was verified that the corrosion becomes more severe as you move from the parent metal to the HAZ (Fang et al., 2024), so more attention should be given to protecting these areas of marine-exposed steel pipes. Figure 11 illustrates that there are both different shapes and various levels of corrosion on the two materials.

Table 1. Comparison of the chemical composition of API X70 Steel

Element	Tested (%)	Certified (%)
C	0.043	0.050
Si	0.149	0.210
Mn	1.51	1.560
P	0.001	0.006
S	<0.003	0.002
Cr	0.228	0.250
Ni	<0.005	0.010
Cu	<0.002	0.010
Al	0.017	0.044
V	0.014	0.030
Mo	0.098	0.160
Ti	0.020	0.020
Nb	0.051	0.070
N	0.004	0.004
Ca	0.0022	0.0022
B	0.0026	0.0004

3.2 Chemical composition analysis

As shown in Table 1, the chemical compositions of API X70 steel have been determined by tests and confirmed in the material certificate. The testing shows that the steel's composition and declared grade are very similar, demonstrating that the grade is genuine. Since the carbon content measured is 0.043% and not even the 0.05% limit, it matches the needs for better weldability and less cracking risk expected from high-strength low-alloy (HSLA) steels. The carbon content is lower, the pipeline becomes more ductile and resistant to damage (Bagarella et al., 2013). Because Mn (1.51%) is found in higher amounts, it improves the solution strength, gets rid of oxygen, and boosts the tensile strength

(Akonyi et al., 2020). Deoxidation and strength in the product are aided by silicon at 0.149% and 0.210% (determined by test and certification).

Since phosphorus levels (P) were below 0.006% tested and 0.002% certified, and sulfur levels (S) were below 0.003% tested and 0.002% certified on both datasets, the values were well within API X70 tolerance levels and ensured the welds remained strong. Very small amounts of niobium (Nb), vanadium (V), titanium (Ti), and molybdenum (Mo) are included to help the structure of the steel and make it stronger. Because of the Nb, the ferrite grain refines to a smaller size during controlled rolling (Zhang et al., 2015). The Al content measured at 0.017% and certified as 0.044% proves that grain refining was done. When added as Cr and Cu, metals are more resistant to corrosion if they are exposed to seawater (Fang et al., 2024). A little bit of boron (B) and calcium (Ca) enhances the toughness of the weld zone (Adedipe et al., 2015). Differences seen in test values and those obtained from certification are within the expected range. API X70 is listed in the elemental profile as HSLA steel and meets the requirements for pipes, resistance to marine corrosion, and weldability as per the API 5L and ISO 3183 standards.

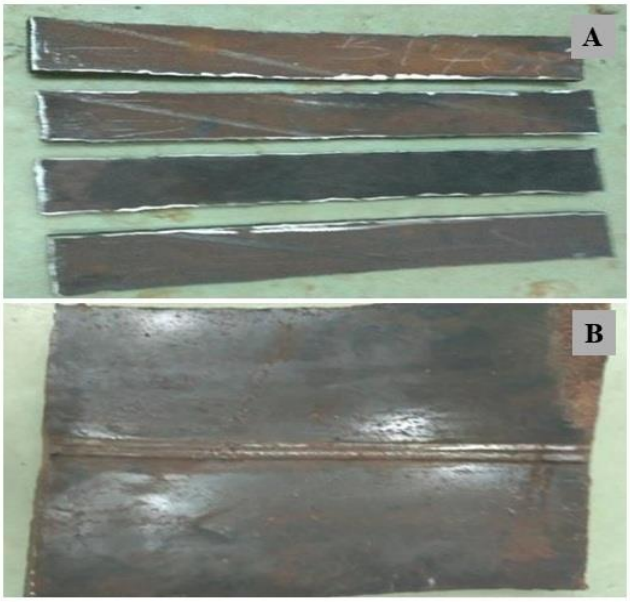

Figure 12. Figure 12. The appearance of API X70 steel plates before welding (A) clean, and each plate faced the other without any welding, while after welding (B), the weld seam and heat-affected surface discoloration when the plates were joined

3.3 Welding: Steel plate before and after welding

AP1 X70 steel plates are displayed in Figure 12 before they are welded and after they are welded. Prepared plates are displayed in Figure 12(A) and do not contain any contaminants. Welds become better if the metal is properly prepared, because impurities may result in fusion defects or porosity. In Figure 12(B), the welded area is apparent and shows a raised weld bead marking the joint. For the thick plates with a 20 mm thickness, the double-V butt joint with 60° groove angle was applied to ensure excellent joint penetration. There are traces of flawless welding, yet the welding process created surface oxidation (Balasubramanian et al., 2009).

Right next to the weld bead, the HAZ should experience grain coarsening and different hardness due to the TMCP nature of API X70 (Lee et al., 2020). According to Adedipe et al. (2015), using incorrect welding parameters can lead to undesirable structures, for instance, having a coarse-grained area (CGHAZ) or a mixture of martensite and austenite (M–A), and that negatively influences the piece's resistance to stress. Kumar et al. (2023) explain that poor management of weld metal in HSLA steel can result in uneven microstructures and might cause failures of pipelines. The weld looks appropriately done, yet an additional assessment is needed to check the metal structure and strength in the welded area.

3.4 Mechanical test results

Tests were done to measure the mechanical qualities of the API X70 steel in all its zones: the parent material, the HAZ, and the weld region, as displayed in the diagram. Such tests explore how the material structure stays secure with welding and with exposure to seawater. The example revealed that from tensile testing, the weld metal had a mean yield strength of 578 MPa, 19 MPa higher than that of the parent material's 560 MPa. This happens because grain refinement and precipitation hardening happen during the solidification and cooling process of welding, as announced by Kumar et al. (2023). After considering the sample weights before and after immersion, it can be noticed that after 12 months in marine water, there was a 126 gram decrease in sample mass as a result of uniform corrosion and pitting (Fang et al., 2024). It seems these results prove that, although weld strength may remain the same or even rise, ongoing corrosion might weaken the weld's ability to resist breaking.

It was shown by Charpy V-notch testing that impact energy absorbency was better in the parent material than in the weld metal or in the HAZ. This trend is predictable since the ferrite–pearlite structure in the parent metal stays the same while in the HAZ, it changes and becomes less tough due to exposure to different heating levels (Kumar et al., 2023). The unevenness in welds and the inclusion of impurities might cause cracks to begin when the material is loaded dynamically. Adedipe et al. (2015) also noticed that the toughness of welded connections drops in marine environments because of unstable structures and cracks instigated by hydrogen. The results of compression testing point out that the maximum load-bearing strength of the parent and the weld area is similar (750.08 MPa and 750.38 MPa, respectively). Nevertheless, the strain and how much energy the parent material could absorb were higher, so it was more capable of bending and dissipating energy. Therefore, while the amount of yield strength does not change, plasticity goes down in the weld zone, probably caused by leftover stress and increased hardness. This happens in agreement with research on HSLA steels, in which welded regions usually have higher strength and less toughness and ductility (Balasubramanian et al., 2009).

The hardness at various parts of the weldment was examined through a reading at 33 chosen locations, as indicated in the schematic picture. Those regions cover 1–11 (weld), 12–22 (heat-affected zone), and 23–33 (raw material). The hardness tends to be greatest at the weld area, because the metal cools down fast and the

grains are finer there, with a decrease towards the heat-affected zone due to bigger grains. Most of the time, the parent rock has a steady and moderately strong hardness. These findings are consistent with the findings of Ike et al. (2018), which indicated that API X70 welds were more likely to suffer from soft areas in the HAZ since their hardness was elevated, thus exposing the components to stress focus when cycled. Altogether, the results show that the welded area gets tougher and stronger, yet it performs worse than the parent material in terms of absorbing impact damage and squeezing loads. Among all areas, the HAZ is the most defenseless, mainly because of dynamic or corrosive loading. This shows that properly carrying out post-weld heat treatment (PWHT) and using proper corrosion protection helps increase the lifespan of such structures in the marine environment.

3.5 Results of SEM analysis

The study used SEM to analyze the fracture surfaces of specimens from the Charpy test to see the nature of failures at the parent material, the weld metal, and the heat-affected zone. Results from air and seawater samples were analyzed to find out the impact of corrosion on the broken structure. The parent material broke in a ductile manner, and its dimples are long, and the tear patterns are fibrous for the sample tested in air (Figure 13). As a result of contact with seawater, the dimples look flatter and include space-filling micropits and small holes, hinting at less plastic deformation and faster microvoid fusion. It means that chloride in the soil for a long time caused hydrogen-assisted embrittlement, which reduced the strength of the specimens, just as Adedipe et al. (2015) and Fang et al. (2024) reported. In weld material, the fracture faces indicate mixed failure, and brittle elements, including cleavage facets and cracks between grains, are observed mostly in the samples exposed to seawater. Microvoids and strange craters in the area mean the fusion zones were not well formed, and the metals became inhomogeneous because of welding heat. According to Kumar et al. (2024), observations from this study show that weld regions of HSLA steels have a higher hardness and also have lower toughness due to the existence of martensite–austenite (M–A) constituents and segregation bands.

The rate of erosion is highest in the HAZ area. SEM pictures demonstrate that there are several points of void formation, cracks spread throughout, and many pores inside the material. The grain coarsening, softening, and zones where some phases appear instead of others cause the HAZ to lose its ability to resist toughness and fatigue. Because of high thermal stress and continual corrosion, the heat-affected zone in welds may fail earlier. These findings in SEM prove that being in seawater reduces the ability of metals to resist fractures, paying special attention to the welded and affected zones. The material in the middle of the ceramic, even though it changes, can flow more and work better in impact and mechanical tests. Morphology of the fracture surface for (top) parent metal, (middle) weld metal, and (bottom) heat-affected zone was studied in an air atmosphere and seawater. Air samples usually have parent material marked by ductile dimples, but the samples exposed to seawater have various signs of pitting and show cracking that explains the failure caused by corrosion.

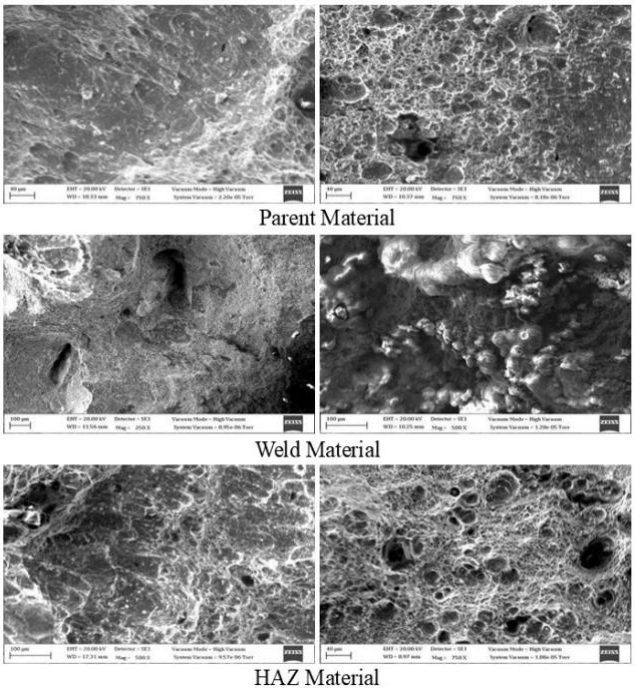

Figure 13. SEM micrographs of fracture surfaces from Charpy specimens of API X70 steel.

4. Conclusion

This study focused on the corrosion of API X70 steel in simulated seawater contributes many insights about how the material works in offshore conditions. Mechanical features found that the yield strength for the parent material in air is 560 MPa, and for the weld is 578 MPa. As for tensile strength, the corresponding values are 634 MPa for the parent material and 674 MPa for the weld. In seawater, the strength of the parent and weld materials went down to 428 MPa and 416 MPa, whereas the tensile strengths were 512 MPa and 529 MPa, respectively. The parent material gave the highest Charpy energy values, the HAZ came in second, and the weld material had the lowest. There was less energy absorption by seawater specimens as compared to air samples. The stress in the structure also decreased because of the water in the seawater. Hardness in the HAZ went from weld to parent metal, and it was highest in the weld (239 HV) and lowest in the parent material (196 HV). Both brittle and ductile ways of breaking could be seen at the fracture surfaces. Seawater corrosion decreased the tensile qualities of the parent material and the weld by 20% and 30%, respectively. It was found that Charpy parent, weld, and HAZ materials suffered a reduction of 2.0 because of seawater. There was a 1.7 and 1.8 reduction in compressive properties due to the presence of seawater in the samples. Environmental reduction is connected to how much time the food is left in the marinade.

References

Abed, A. A. S. (2021). Influence of ZnO nano-refrigerant in R134a on performance compression systems of refrigeration.

Periodicals of Engineering and Natural Sciences (PEN), 9(3), 734-744.

Adedipe, O. (2015). "Integrity of Offshore Structures." PhD Thesis, Cranfield University.

Adedipe, O., Gambo, A. B., Abutu, J., Olugboji, O. A., Babalola Agboola, J., Obanimomo, K. T., & Abdulrahman, A. S. (2023). An evaluation of mechanical properties and estimation of environmental reduction factors in welded API X70 steel pipeline in natural seawater. Welding International, 37(5), 269-281.

Akonyi, N. S., Olugboji, O. A., Egbe, E. A. P., Adedipe, O., & Lawal, S. A. (2020). Optimisation of process parameters for MAG welding of API X70m material to predict tensile strength using Taguchi method. Nigerian Journal of Technology, 39(4), 1100-1107.

Aliu, S. (2012). Investigation of mechanical and microstructural properties of welded joint of Nigerian National Petroleum Corporation pipelines. M. Eng, Thesis, Federal University of Technology Minna, Nigeria, 9-15.

Bagarella, G., Lazzarin, R. M., & Lamanna, B. (2013). Cycling losses in refrigeration equipment: An experimental evaluation. International Journal of Refrigeration, 36(8), 2111-2118.

Behera, B., Unpaprom, Y., Ramaraj, R., Maniam, G. P., Govindan, N., & Paramasivan, B. (2021). Integrated biomolecular and bioprocess engineering strategies for enhancing the lipid yield from microalgae. Renewable and Sustainable Energy Reviews, 148, 111270.

Balasubramanian, V., Varahamoorthy, R., Ramachandran, C. S., & Muralidharan, C. (2009). Selection of welding process for hardfacing on carbon steels based on quantitative and qualitative factors. The International Journal of Advanced Manufacturing Technology, 40, 887-897.

Bhuyar, P., Rahim, M. H. A., Sundararaju, S., Ramaraj, R., Maniam, G. P., & Govindan, N. (2020). Synthesis of silver nanoparticles using marine macroalgae Padina sp. and its antibacterial activity towards pathogenic bacteria. Beni-Suef University Journal of Basic and Applied Sciences, 9, 1-15.

Bott, I. S., Siciliano, F., Batista, G. Z., & Gray, J. M. (2024). Line Pipe Steels. In Handbook of Pipeline Engineering (pp. 285-310). Cham: Springer International Publishing.

Fang, X., Wu, Y. X., Yang, X. Y., Yang, Y. G., Cheng, L., Zhang, Q., ... & Mi, Z. L. (2024). Microstructure and mechanical properties of the laser welded air-hardening steel joint. Materials Characterization, 213, 114048.

Gambo, A. B. (2022). investigation on the effects of seawater on mechanical properties of api 5l x70 steel pipeline weldment (Doctoral dissertation).

Govindan, N., Maniam, G. P., Yusoff, M. M., Ab. Rahim, M. H., Chatsungnoen, T., Ramaraj, R., & Chisti, Y. (2020). Statistical optimization of lipid production by the diatom Gyrosigma sp. grown in industrial wastewater. Journal of Applied Phycology, 32, 375-387.

Hwang, B., Kim, Y. M., Lee, S., Kim, N. J., & Ahn, S. S. (2005). Correlation of microstructure and fracture properties of API X70 pipeline steels. Metallurgical and Materials Transactions A, 36, 725-739.

Ike, T. M., Adedipe, O., Abolarin, M. S., & Lawal, S. A. (2018). Mechanical characterization of welded API X70 steel exposed to air and seawater: a review. In IOP Conference Series: Materials Science and Engineering, IOP Publishing 413 (1), 012034.

Jayabalan, R. (2019). Seawater–a sustainable solution for the freshwater drain in bioethanol industries. Maejo International Journal of Energy and Environmental Communication, 1(2), 20-25.

Kumar, N., Kumar, P., Upadhyaya, R., Kumar, S., & Panday, C. (2023). Assessment of the structural integrity of a laser weld joint of Inconel 718 and ASS 304L. Sustainability, 15(5), 3903.

Lawal, S. L., Afolalu, S. A., Jen, T. C., & Akinlabi, E. T. (2024). Corrosion Control and its Application in Marine Environment-A Review. Solid State Phenomena, 355, 61-73.

Lee, C. S., Chandel, R. S., & Seow, H. P. (2000). Effect of welding parameters on the size of heat affected zone of submerged arc welding. Materials and Manufacturing Processes, 15(5), 649-666.

López, M., Claus, R., Soto, F., Hernández-Garrastacho, Z. A., Cebada-Relea, A., & Simancas, O. (2024). Advancing offshore solar energy generation: The HelioSea concept. Applied Energy, 359, 122710.

Louhenkilpi, S. (2024). Continuous casting of steel. In Treatise on process metallurgy (pp. 343-383). Elsevier.

Sabarikirishwaran, P., Shen, M. Y., Ramaraj, R., Unpaprom, Y., Wu, H. C., & Chu, C. Y. (2023). Feasibility and optimizing assessments on biogas and biomethane productions from E. coli fermenter effluent. Biomass and Bioenergy, 173, 106783.

Seth, D., Manna, B., & Shahu, J. T. (2024). On-bottom stability of a radial fin integrated surface-laid pipe-section against vertical penetration. Applied Ocean Research, 151, 104165.

Song, J., Zhang, H., Yin, C., Chen, J., Yu, W., Zhou, H., ... & Xiao, K. (2024). Study on initial corrosion behavior of bogie steels with ferrite+ pearlite and granular bainite structures immersed in sulfur-containing environment. Journal of Materials Research and Technology, 29, 2188-2203.

Suliman, A. A. M., Isha, R., Seman, M. N. A., & Ahmad, A. L. (2020). Synthesis and characterization of TiO2 and palm oil fiber ash hybrid photocatalysts for seawater pretreatment. Maejo International Journal of Energy and Environmental Communication, 2(3), 11-20.

Ujjwal, K., Al-Saadi, S., Das, A. K., & Raman, R. S. (2024). Corrosion and stress corrosion cracking characteristics of 4043 aluminium alloy fabricated through directed energy deposition process. Journal of Alloys and Compounds, 976, 173154.

Xia, D., Okada, K., Watanabe, K., Miura, Y., Ramaraj, R., Wangchai, N., ... & Itayama, T. (2018a). Role of sulphide reduction by magnesium hydroxide on the sediment of the eutrophic closed bay. Aquaculture Research, 49(1), 462-470

Xia, D., Okano, K., Miura, Y., Ramaraj, R., & Itayama, T. (2018b). The effects of magnesium hydroxide for the microbial community in the sediments of a eutrophic closed bay. Geomate Journal, 14(41), 143-150.